

Manuscript version: Author's Accepted Manuscript

The version presented in WRAP is the author's accepted manuscript and may differ from the published version or Version of Record.

Persistent WRAP URL:

<http://wrap.warwick.ac.uk/110578>

How to cite:

Please refer to published version for the most recent bibliographic citation information. If a published version is known of, the repository item page linked to above, will contain details on accessing it.

Copyright and reuse:

The Warwick Research Archive Portal (WRAP) makes this work by researchers of the University of Warwick available open access under the following conditions.

Copyright © and all moral rights to the version of the paper presented here belong to the individual author(s) and/or other copyright owners. To the extent reasonable and practicable the material made available in WRAP has been checked for eligibility before being made available.

Copies of full items can be used for personal research or study, educational, or not-for-profit purposes without prior permission or charge. Provided that the authors, title and full bibliographic details are credited, a hyperlink and/or URL is given for the original metadata page and the content is not changed in any way.

Publisher's statement:

Please refer to the repository item page, publisher's statement section, for further information.

For more information, please contact the WRAP Team at: wrap@warwick.ac.uk.

Stellar flare oscillations: Evidence for Oscillatory Reconnection and Evolution of MHD Modes

J.G. Doyle¹  J. Shetye^{1,3} A.E. Antonova² D. Y. Kolotkov³ A.K. Srivastava⁴
M. Stangalini⁵ G.R. Gupta⁶ A. Avramova² M. Mathioudakis⁷

¹ Armagh Observatory and Planetarium, College Hill, Armagh BT61 9DG, N. Ireland

² Department of Astronomy, Faculty of Physics, St Kliment Ohridski University of Sofia, 5 James Bourchier Boulevard, 1164 Sofia, Bulgaria

³ Centre for Fusion, Space and Astrophysics, Department of Physics, University of Warwick, CV4 7AL, UK

⁴ Department of Physics, Indian Institute of Technology (Banaras Hindu University), Varanasi-221005, India

⁵ INAF-OAR National Institute for Astrophysics, 00078, Monte Porzio Catone, RM, Italy

⁶ Inter-University Centre for Astronomy and Astrophysics, Post Bag-4, Ganeshkhind, Pune 411007, India

⁷ Astrophysics Research Centre, School of Mathematics and Physics, Queen's University Belfast, BT7 1NN, N. Ireland

Accepted XXX. Received YYY; in original form ZZZ

ABSTRACT

Here, we report on the detection of a range of quasi-periodic pulsations (20 – 120s; QPPs) observed during flaring activity of several magnetically active dMe stars, namely AF Psc, CR Dra, GJ 3685A, Gl 65, SDSS J084425.9+513830 and SDSS J144738.47+035312.1 in the GALEX NUV filter. Based on a solar analogy, this work suggests that many of these flares may be triggered by external drivers creating a periodic reconnection in the flare current sheet or an impulsive energy release giving rise to an avalanche of periodic bursts that occur at time intervals that correspond to the detected periods, thus generating QPPs in their rising and peak phases. Some of these flares also show fast QPPs in their decay phase, indicating the presence of fast sausage mode oscillations either driven externally by periodic reconnection or intrinsically in the post-flare loop system during the flare energy release.

Key words: stars: flare – stars: activity – stars: late-type – ultraviolet: stars – waves – magnetohydrodynamics

1 INTRODUCTION

Flare light-curves often show an oscillatory pattern, referred to as quasi-periodic pulsations (QPPs). More specifically, some QPPs exhibit periodic and decaying variation of the flux in a particular wave band after the flare peak, while others are only present in the impulsive phase. For solar flares these range from milli-seconds to a few minutes, while stellar flares can have oscillations of up to several tens of minutes (Welsh et al. 2006; Cho et al. 2016; Simões et al. 2015). If QPPs are generated by quasi-periodic processes, then this provides information on the on-going physical processes during the flare, e.g., evolution of MHD mode(s) or periodic reconnection and thus associated energy release as well as modulation of emission (Mitra-Kraev et al. 2005; Nakariakov 2007; Van Doorselaere et al. 2016). Some authors, e.g. Russell & Fletcher (2013), have even suggested that MHD waves may be responsible for energy transport from the reconnection region to the flare foot-points contradicting the conventional thick-target model. Three possible

mechanisms exist: the oscillations are excited by the external flare trigger, within the flare itself, or in post-flare loops (Mathioudakis et al. 2003, 2006; Pandey & Srivastava 2009; McLaughlin et al. 2012; Srivastava et al. 2013; Pucci et al. 2014). The signature of QPPs is a very important tool, allowing us to gain an insight into the physical conditions within the stellar atmospheres. Recent observations have detected super-flares in the lower atmosphere of magnetically active stars (Maehara et al. 2012; Anfinogentov et al. 2013). Balona et al. (2015) performed a study of QPPs in the white light emission from stellar flares based on Kepler data. Multi-periodic QPPs are also detected in many flares (Pugh et al. 2015). Although the modulation in the white light emissions gives information about the physical processes occurring in the stellar flares near the surface of the star, similar QPPs observed in X-ray or UV describe the localised physical conditions higher in the atmosphere, e.g. chromosphere or corona. Recently, Srivastava et al. (2013) observed the presence of multiple harmonics of slow magneto-acoustic oscillations in an X-ray flare on Proxima Centauri, and performed MHD seismology. They measured the density scale height of its corona to be smaller than the

* E-mail: jgd@arm.ac.uk

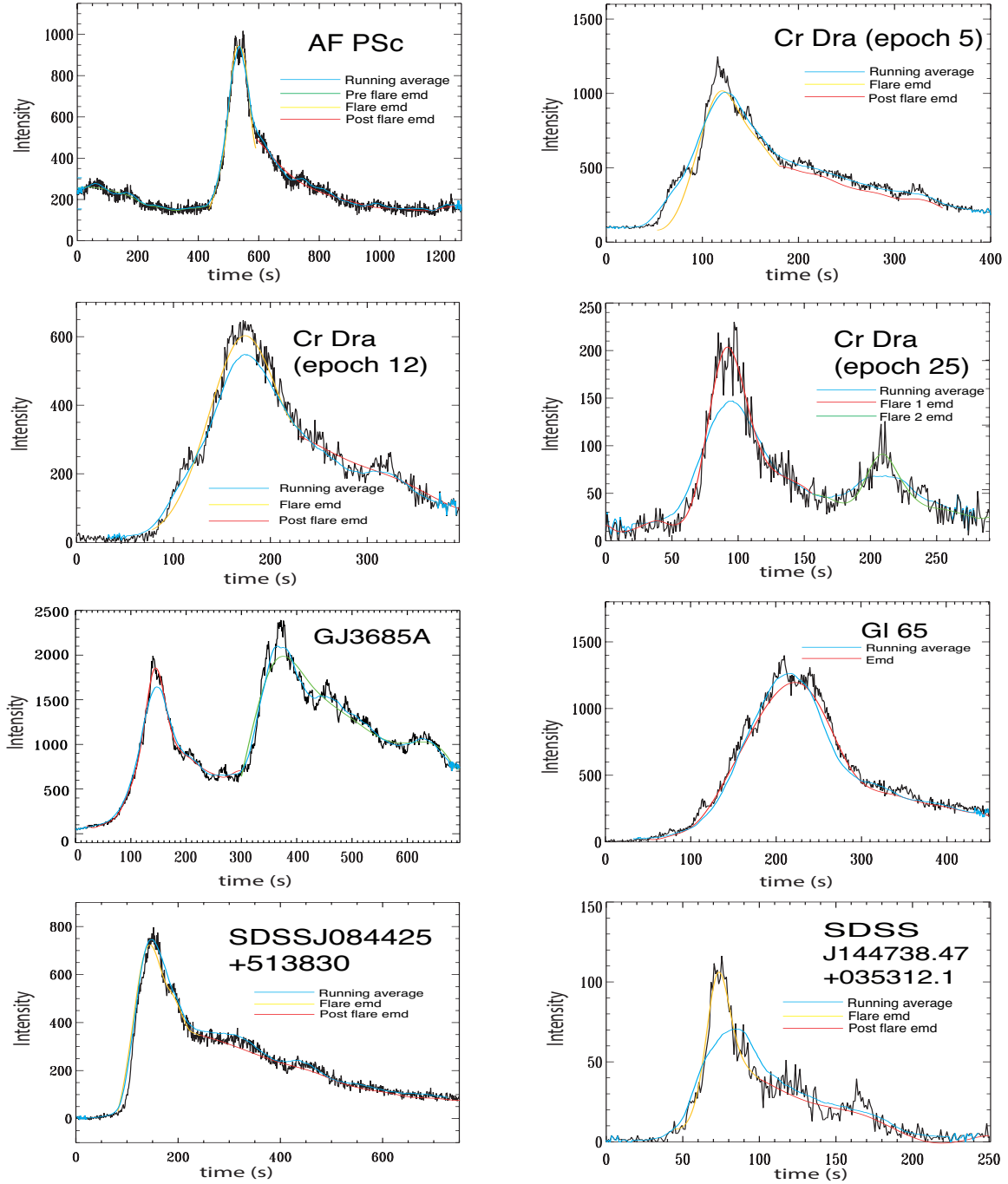


Figure 1. The flare light-curves for AF Psc, CR Dra, GJ 1167A, GJ 3685A, Gl 65, SDSS J0844+5138 and SDSS J144738.47+035312.1 as seen in the NUV/Galex filter. The "0" on the x-axis corresponds to start time given in Table 1. We show three flares from CR Dra which we label epoch 5, 12 and 25. For each flare we over-plot the overall trend in the flare light-curve as estimated using a running mean and the empirical mode composition.

typical hydrostatic scale height, and indicated the presence of non-equilibrium conditions there.

Cho et al. (2016) looked at QPPs in solar flares with RHESSI and stellar flares using XMM data. Typical periods derived from stellar flares are 16.2 ± 15.9 min with a damping time of 27.1 ± 28.7 min., while for solar flares the

QPPs period was 0.9 ± 0.6 min with a damping time of 1.5 ± 1.1 min. The interesting finding of this work was that the ratio of the damping time (τ) to period (P) was 1.59 for stellar flares and 1.74 for solar events. In-fact, a straight line fit of $\tau = 1.62P^{0.99}$ fitted QPPs ranging in period from ~ 20 s to 60 min, suggesting a similar mechanism.

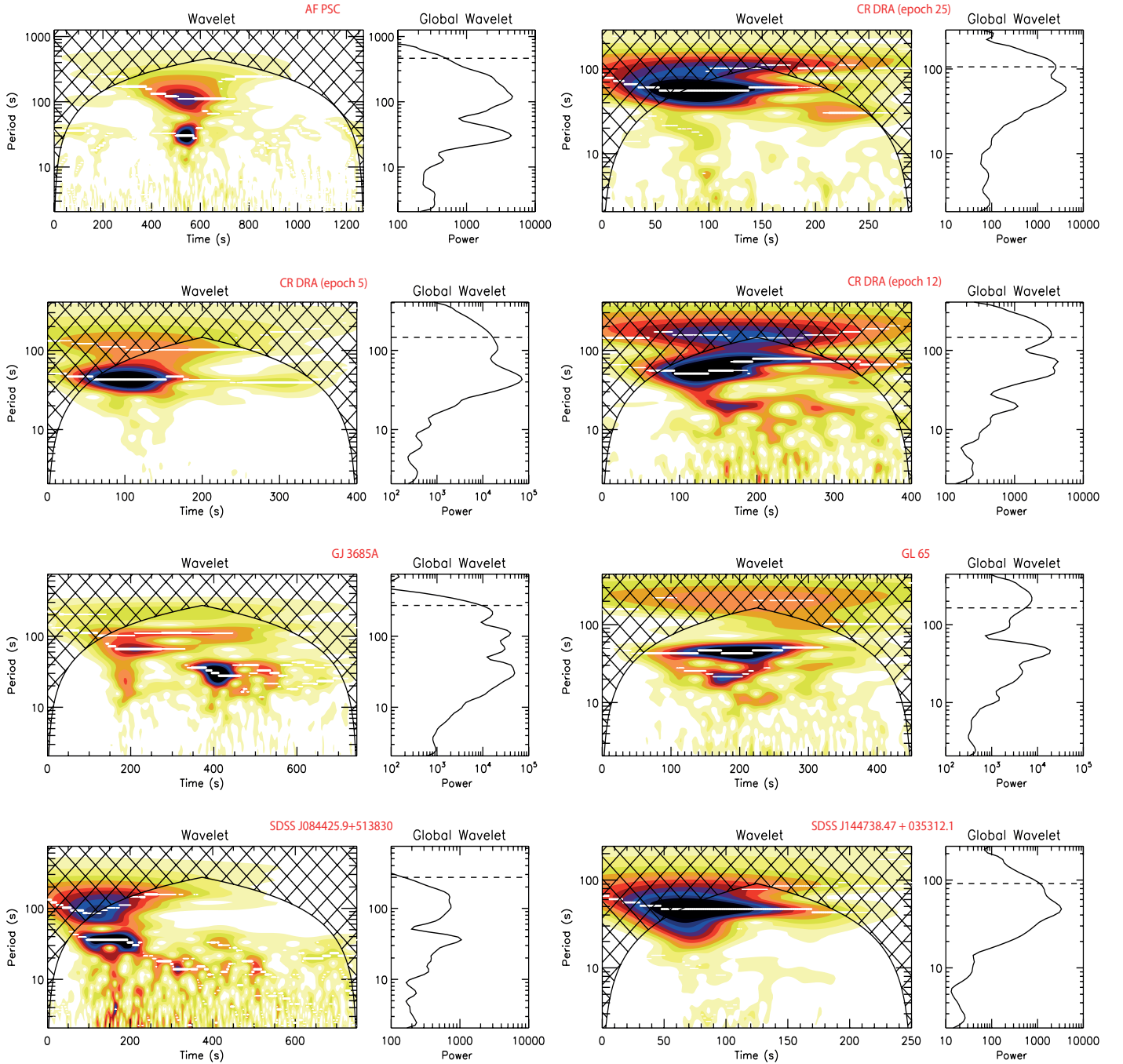


Figure 2. Wavelet intensity spectrum of the flares for AF Psc, CR Dra, GJ 3685A, Gl 65, SDSS J084425.9+513830 and SDSS J144738.47+035312.1 based on the boxcar de-trended data, showing dominant periodicities with the global wavelet.

Here, we extend work first presented by [Welsh et al. \(2006\)](#) which used data from GALEX. The GALEX satellite ([Martin et al. 2005](#)) was launched in 2003 and operated for just over 10 years. Although its primary mission was to study galaxies, it proved to be an excellent observatory for the serendipitous detection of stellar flares. It operated in two ultraviolet wavebands: the far UV (FUV: 1350 – 1750 Å) and/or near UV (NUV: 1750 – 2800 Å) and was capable of providing sub-second time resolution data of flares. In addition to looking again at the oscillations reported by [Welsh et al. \(2006\)](#) we include additional objects, plus we searched for evidence of additional periods in the data as

done by [Van Doorselaere et al. \(2011\)](#). For this, we used two different techniques, wavelet transformation **plus** the empirical mode decomposition addressing different issues; how many of these UV flares on M dwarfs show oscillations, when during the flare do we see them, do we see more than one period during the flare and is there evidence for period evolution during the flare?.

[Welsh et al. \(2006\)](#) looked at the line and continuum contribution in the NUV filter (for a non-flaring atmosphere). The dominant line emitters were Mg II, Fe II, Al III, C III, etc. For example, Mg II has ~10% contribution, the region from 2320 to 2530Å contributes ~17% (mostly Fe

ii), while the lines around $2290 \pm 20\text{\AA}$ supplies $\sim 14\%$. The remaining NUV flux contribution arises from the various continuum processes. Thus emission observed in this filter originates mostly in the upper chromosphere/lower transition region.

2 OBSERVATIONS

The flares were identified and light curves were produced using the gPhoton database and modules (Million et al. 2016). gPhoton is a GALEX data calibration and extraction pipeline that allows easy access to time-tagged photon events. After identifying the available exposures for a number of M dwarfs, we generated count maps for each star and epoch. We used these to find flare events and determine the coordinates, aperture and background annulus size and position, the latter to make sure that a contaminating sources was not present. These parameters were used to obtain the calibrated time-tagged data with a time resolution of 1s. In the following sections we present the results and analysis of the brightest flares found. Light curves were obtained for flares from AF Psc, CR Dra, GJ 1167A GJ 3685A, GJ 65, SDSS J084425+513830 and SDSS J144738.47+035312.1 in the NUV filter and are shown in Fig. 1. Since gPhoton is still experimental, we compared these flare light curves with those published in Welsh et al. (2006), using the same aperture (10 arcsec aperture) and background annulus (extending from ~ 15 to 20 arcsec from the central position of the star). Excellent agreement was obtained for AF Psc, CR Dra (epoch 5) and SDSS J084425+513830, while GJ 3685A differed by $\sim 20\%$.

3 ANALYSIS AND OBSERVATIONAL RESULTS

We extracted the periods using two different methods, a boxcar de-trending followed by wavelet and the empirical mode decomposition.

3.1 Wavelet

Before using the wavelet, the light-curves were de-trended using a running mean. We tested values ranging from 40s to 60s, but no difference was apparent in the resulting de-trended light-curve. The signal is a time-series of length t consisting of data points spanning over an interval δt and the total length as $N\delta t$. The output of the wavelet procedure is a relation between the Fourier Frequency t^{-1} to the time-step $(2\delta t)^{-1}$. For such a time-series, the Morlet wavelet consisting of a plane wave modulated by a Gaussian is given by Torrence & Compo (1998).

$$\Psi_0(\eta) = \pi^{-1/4} e^{i\omega_0\eta} e^{-\eta^2/2} \quad (1)$$

where ω_0 is a non-dimensional frequency. A continuous wavelength transform for a discrete time series x_n is derived by convolution of x_n with δt . Here we use scaled and translated version of $\Psi_0(\eta)$. The waveform is given by :

$$W_n(s) = \sum_{n'=0}^{N-1} x_{n'} \Psi^* \left[\frac{(n' - n)\delta t}{s} \right] \quad (2)$$

where s is the wavelet scale, n is localised time and Ψ^* is a complex conjugate of Ψ . Further, the convolution discussed in eq. 2 is carried out for N number of points in the time-series. We carry these N convolutions simultaneously in Fourier space using a discrete Fourier Transform (DFT) given by

$$\hat{x}_k = \frac{1}{N} \sum_{n=0}^{N-1} x_n e^{\frac{-2\pi i k n}{N}} \quad (3)$$

where $k = 0$ to $N - 1$ is the frequency index (in a continuous case the Fourier transform of a function $\Psi(t/s)$ is given by $\hat{\Psi}(s(\omega))$). Thus the wavelet transform is :

$$W_n(s) = \sum_{k=0}^{N-1} \hat{x}_k \hat{\Psi}^*(s(\omega_k)) e^{i\omega_k n \delta t} \quad (4)$$

The angular frequency is given by ω_k and has limits $\pm 2\pi k/N\delta t$. Thus a continuous wavelet transform can be computed using eq. 4 and a standard Fourier transform routine.

Wavelet plots for some of these flares were shown in Welsh et al. (2006), below, we summarize the results for each flare based on both analyses (see Fig. 2)

AF Psc: From the wavelet, a period of 30s is apparent in the late rise phase/flare peak, plus a longer period of ≈ 120 s throughout the flare. There was no evidence of additional periods in the decay phase.

CR Dra (epoch 5): From the wavelet, a period of 43s was apparent from just before flare peak to late in the decay phase.

CR Dra (epoch 12): From the wavelet, this flare showed two periods, 43s in the rise phase followed by a 20s in the decay phase.

CR Dra (epoch 25) There are two periods in the impulsive/flare peak of 60s and ~ 100 s.

GJ 3685A: This star produced two flares separated by a few minutes. From the wavelet, three periods were apparent in the data; a period of 110s throughout both flares, a period of 60s during the first flare and a period of 36s during the early part of the second flare.

GJ 65: Again, this flare showed two periods based on the wavelet, 46s in the rise phase to late in the decay phase with a weak ~ 25 s period around flare maximum.

SDSSJ084425+513830: From the wavelet, this flare showed two periods of 40s and 120s around flare peak.

SDSSJ144738.47+035312.1: This flare had a 48s period throughout its short decay phase based on the wavelet.

3.2 Empirical Mode Decomposition

Born as a preconditioning technique for the Hilbert transform, the EMD method moves from the assumption that a time series, representing a physical process, is the superposition of many active time-scales, and decomposes the signal into a series of intrinsic mode functions (IMFs). Unlike other techniques (e.g. based upon fast Fourier transform), this decomposition basis is not set *a priori* but locally defined starting from the signal itself. This fact makes the

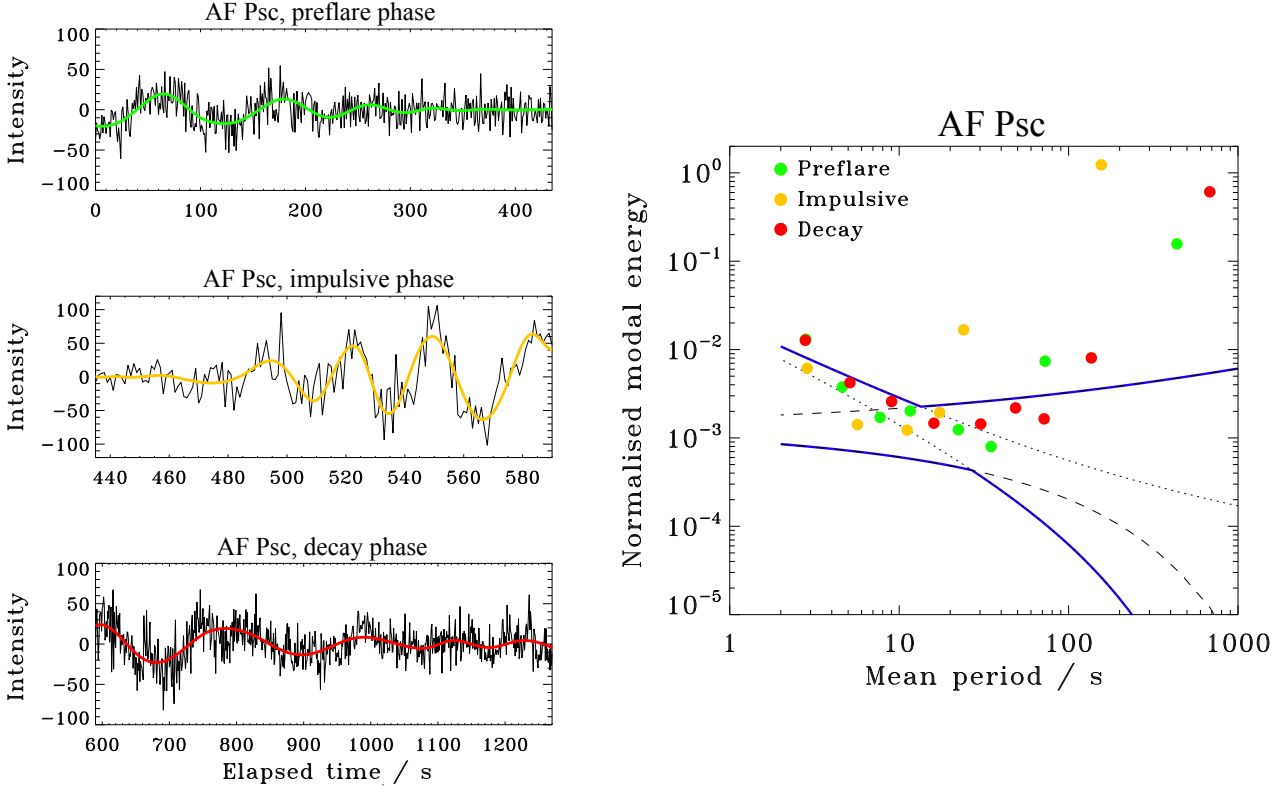


Figure 3. EMD results for AF Psc showing the derived periods for the pre-flare, impulsive phase and decay phase super-imposed on the EMD de-trended light-curve, plus the significance of the derived signals. The dotted and dashed lines are the confidence intervals of the white and pink noises separately, while the blue lines show their superposition, i.e. overall confidence interval.

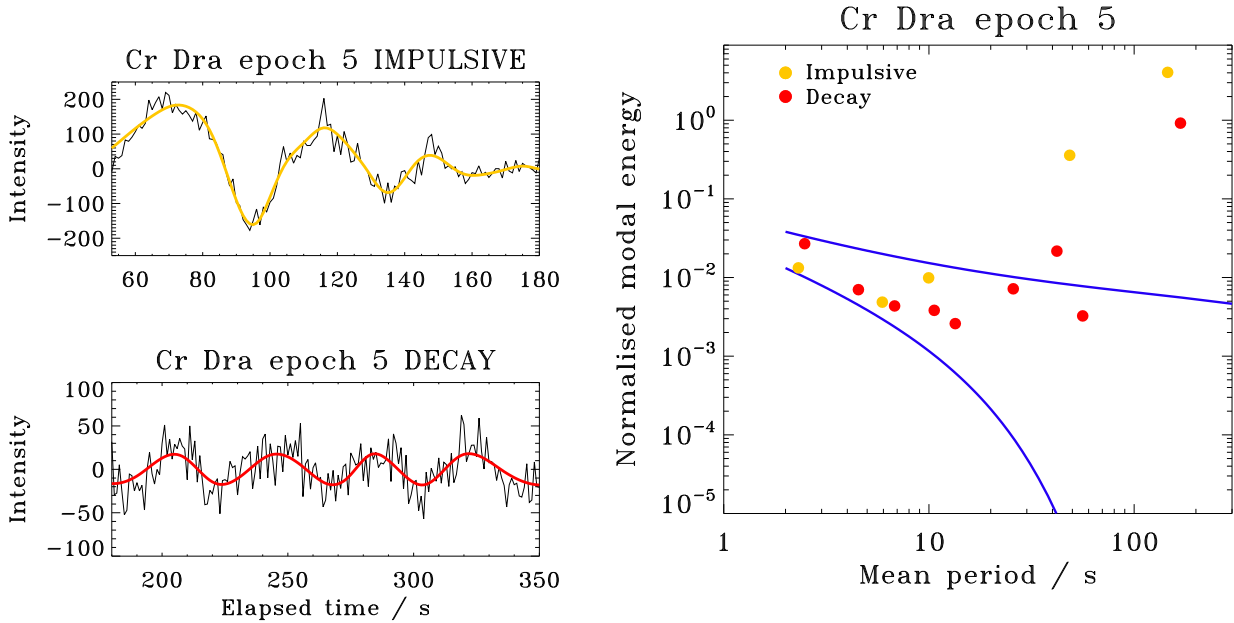


Figure 4. EMD results for CR Dra (epoch 5) showing the derived periods for the impulsive and decay phase, plus the significance of the derived signals.

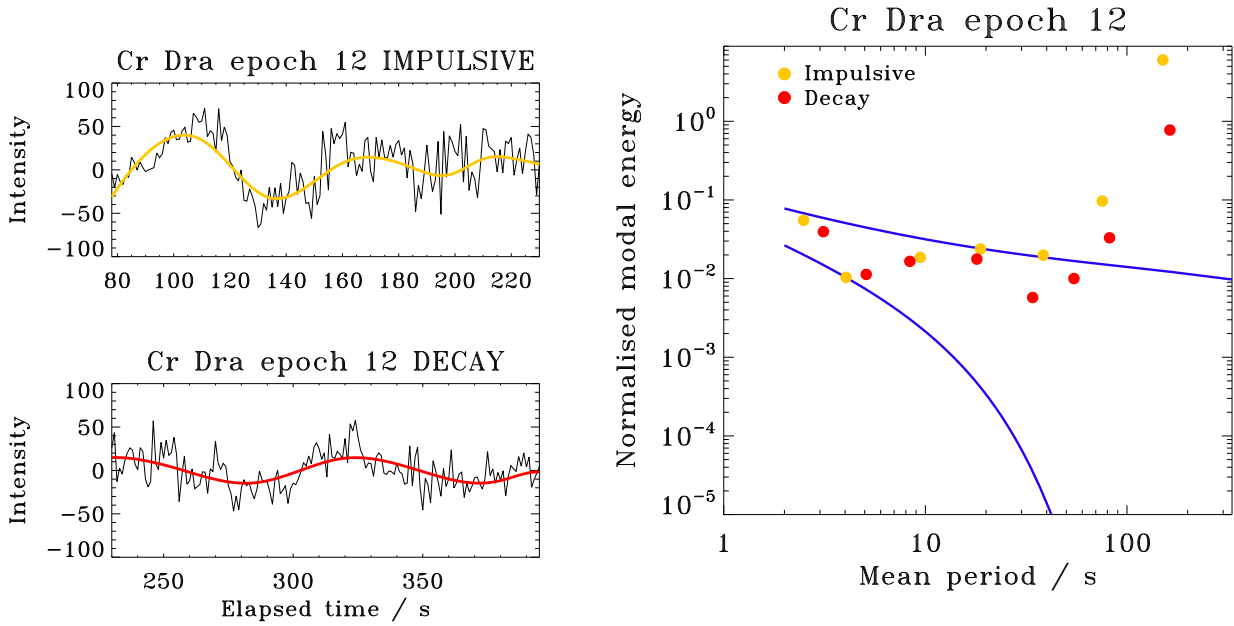


Figure 5. EMD results for CR Dra (epoch12) showing the derived periods for the impulsive and decay phase, plus the significance of the derived signals.

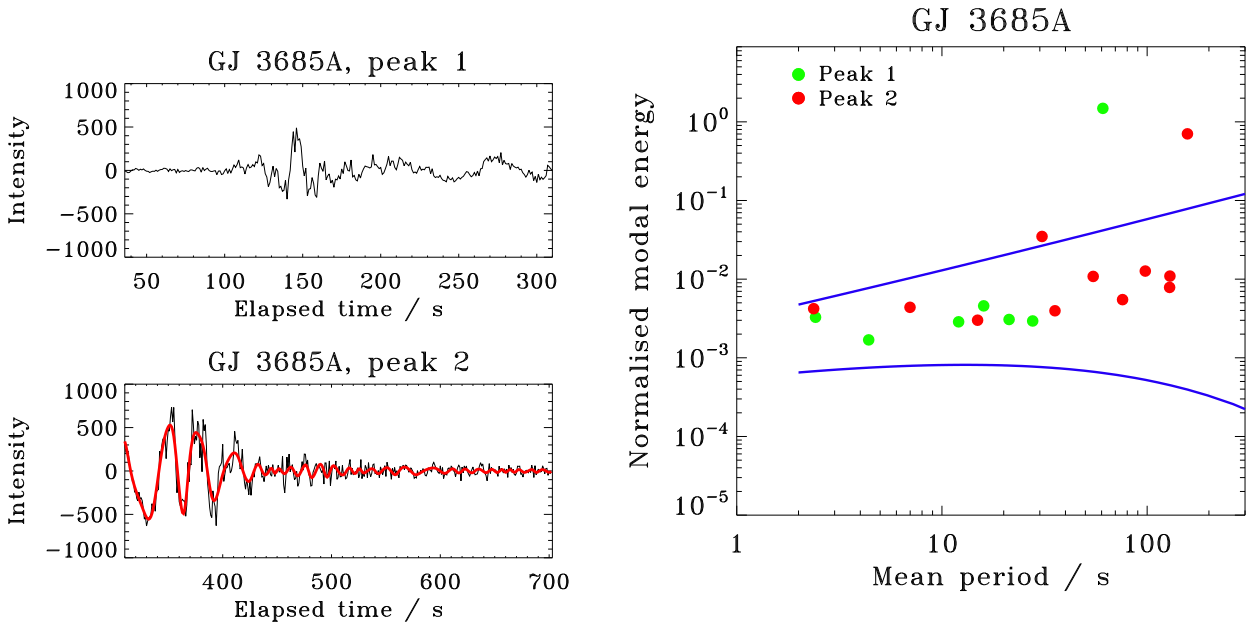


Figure 6. EMD results for GJ 3685A showing the derived periods for the peaks of the two flares as seen in Fig. 1, plus the significance of the derived signals.

technique suited to the study of non-stationary and non-linear processes. Each IMF is obtained by estimating the upper and lower envelopes of a signal $I(t)$, calculating their average $e(t)$, and defining a new time series as the difference $I(t) - e(t)$. The first IMFs contains the high-frequency content of the original signal, while the last few IMFs contain the low-frequency part. This feature can be used to filter out the low frequency part of a signal. Indeed, by summing up several of the higher order IMFs one obtains a de-trended

version of the original signal. The number of IMFs considered depends on the specific needs. Here we have used a different number of IMFs for each flare. This number is found by a visual inspection of the filtered time-series.

For the EMD, we considered all the signals as a combination of a smooth trend (flare itself), statistically significant oscillation plus randomly distributed background. The latter is represented by coloured noises characterised by the power law index α in the dependence of their

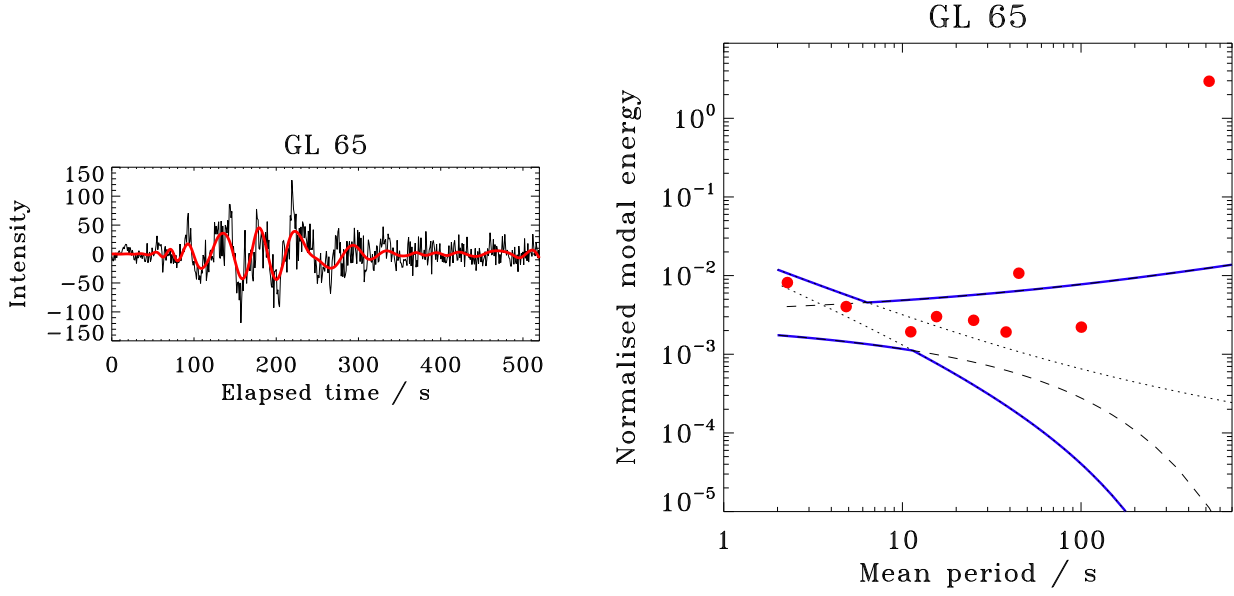


Figure 7. EMD results for GL 65 showing the derived periods using the whole flare interval as shown in Fig. 1, plus the significance of the derived signals.

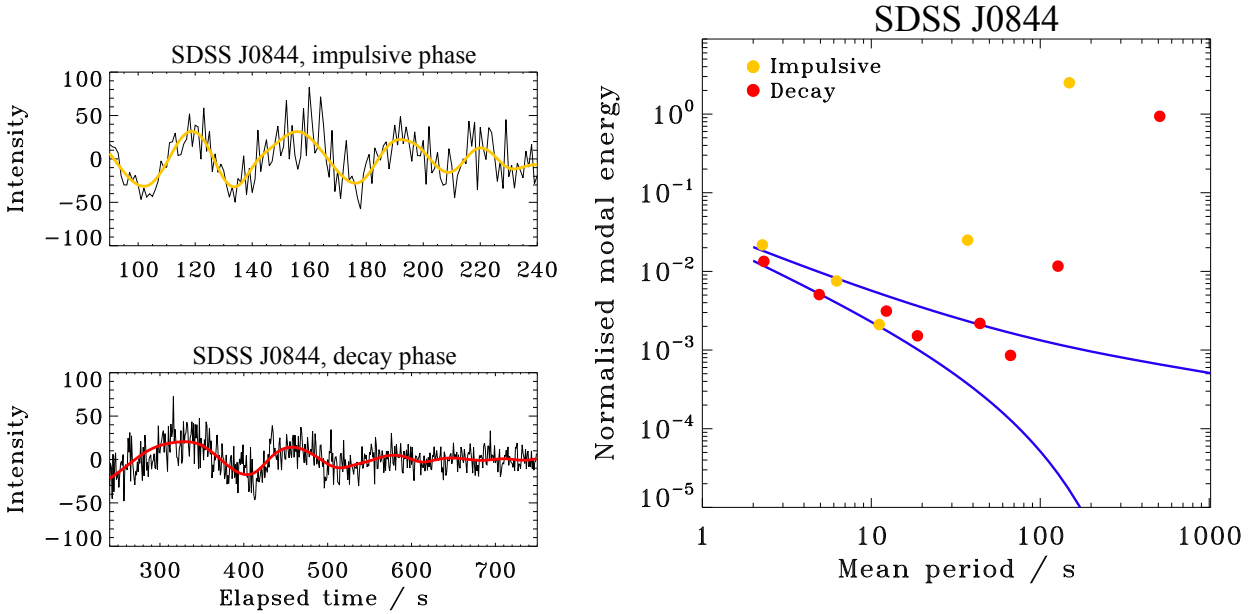


Figure 8. EMD results for SDSS J084425.9+513830 showing the derived periods for the impulsive and decay phases, plus the significance of the derived signals.

Fourier spectral power S upon the frequency f , $S \sim 1/f^\alpha$. In the context of the EMD approach, it is re-written as $E \times P^{(1-\alpha)} = \text{const}$, where E is the EMD modal energy, and P is the main modal period. For instance, $\alpha = 0$ corresponds to the case of white noise (with constant Fourier power S and $E \times P = \text{const}$), $\alpha = 1$ is the pink (flicker) noise. Kolotkov et al. (2016) developed the EMD technique in the presence of coloured noise, allowing for clear distinguishing between quasi-periodic oscillatory phenomena in

the solar atmosphere and superimposed random background processes; these results are given below with the derived periods given in the final plot for each flare.

It is a standard practise to distinguish several phases of a typical solar flare according to the timing of the emission recorded in different bands, e.g. see Benz (2008). Consequently and based upon the analogy between solar and stellar flares, one may naturally expect different physical mechanisms to dominate during different phases of a stel-

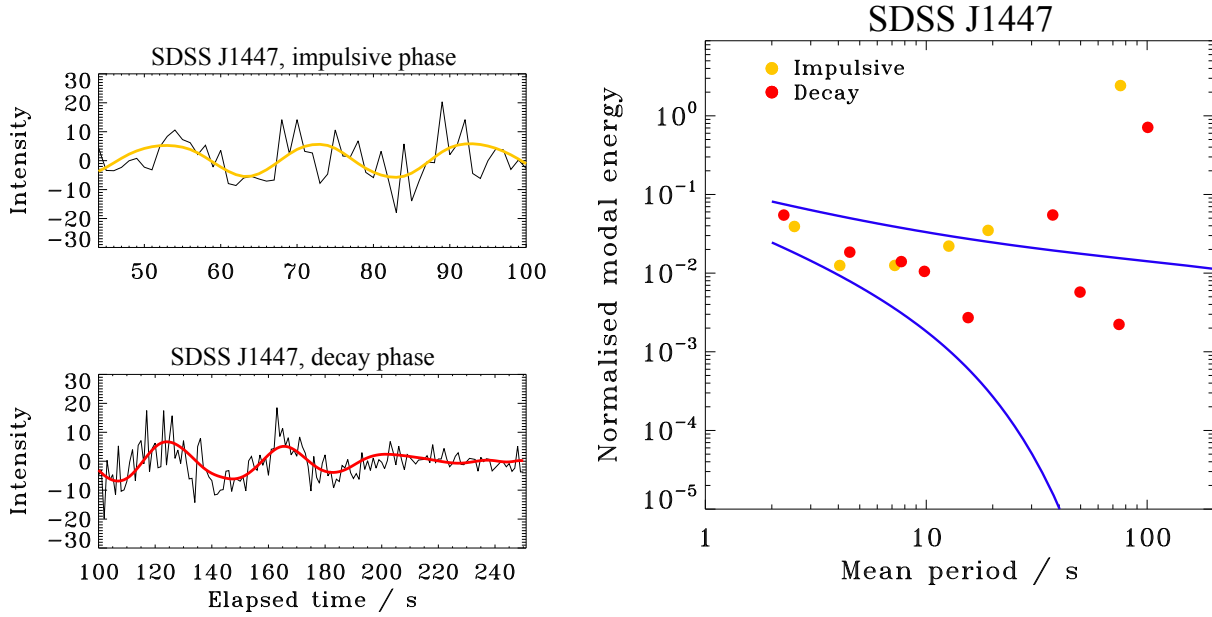


Figure 9. EMD results for SDSS J144738.47+035312.1 showing the derived periods for the impulsive and decay phases, plus the significance of the derived signals.

lar flare too, e.g. coronal loop oscillations before and after the flare and (repetitive) reconnection during it. These processes are entirely different and hence may have substantially different periodicities, which can mix up and produce meaningless results in a spectral analysis if an entire flare is considered. The latter justifies the split of a flare light-curve into a number of phases. In our analysis, we split the light-curves into pre-flare, impulsive, and decay phases. The start and end time of each phase have been chosen manually and empirically according to the general behaviour of the light-curve (i.e. of their gradients/local slopes). More specifically, the pre-flare phase is the light-curve prior to a flux increase due to the flare, the impulsive phase is from flare onset to an apparent break in the gradient of a light-curve after flare maximum (according to the empirical template proposed by [Davenport et al. \(2014\)](#)), and flare decay is the rest of a light-curve until the end of the flux increase as seen in Fig. 1. On the other hand, simultaneous multi-frequency stellar flare observations are generally unavailable, so we have nothing to compare with for a more rigorous comparison. Such a split leads to a reduction of the length of the analysed time series, however, it does not corrupt the results of an EMD analysis and does not contradict common sense, as the method operates locally and self-adaptively and thus does not care about the length of the analysed signal.

We found the signal to consist of the superposition of the white (Fourier spectral energy is constant) and pinkish (Fourier spectral energy is proportional to $1/f$) noises (see Figs. 3–9), as well as oscillatory modes with statistically significant properties. The significant level was set to 99%.

AF Psc: The light-curve consists of the overall flare-trend, a combination of the white (at shorter periods) and pink (at longer periods) noisy components (with breaking point in the vicinity of 15s), and three statistically significant

oscillations in the pre-flare, impulsive, and decay phases, respectively. In the impulsive phase the mode has a stable period of 25s with a growing amplitude. In the pre-flare phase we found a period of ~ 80 s, while in the decay-phase the period was 120s, decreasing with amplitude (see Fig 3). This could be the reason why we did not detect the latter **using the wavelet**. The confidence intervals (given in the right-hand panel) of the combined effect of the white and pink noise are given by the blue lines. We also show in this figure the detected oscillations **over-plotted** on the observational data.

CR Dra (epoch 5): It is well described by the model of white noise ($\alpha \approx 0$, see the corresponding confidence intervals in the spectrum plot, shown in blue in Fig 4), smooth trends (two points in the top right corner of the spectrum plot) and two statistically significant oscillations in the impulsive (50s) and decaying (40s) phases (the other two points are above the noise confidence interval in the spectrum plot).

CR Dra (epoch 12): Same as for the previous case: white noise, trends, and two periodicities in the impulsive (70s) and decaying (80s) phases with statistically significant properties (see Fig 5). However, the signal to noise ratio in the impulsive phase of this flare seems to be lower than that of CR Dra epoch 5. There are two additional periods in the impulsive phase of 20s and 40s which are just on the significance level.

CR Dra (epoch 25): Both peaks are well described by the white noise and smooth trends, with NO significant oscillations, although there is a 30s oscillation just below the 99% significant level for the second flare. This lack of a period is in disagreement with the wavelet.

GJ 3685A: Both flare peaks have smooth trends and reddish ($\alpha \approx 1.5$) noisy component which dominates at longer periods, with a 30s oscillation in the second flare.

see Fig 6. We do not detect the longer periods as seen in the wavelet.

G1 65: Here we have pink ($\alpha \approx 1$) noise plus a smooth trend, and one statistically significant oscillation of ~ 40 s, see Fig 7.

SDSS J084425.9+513830: In addition to the white noise, plus the smooth trend, we have two significant oscillations in the impulsive (35s) and decay (120s) phases (see Fig 8).

SDSS J144738.47+035312.1: Again we have white noise plus a smooth trend, and two significant oscillations in the impulsive (20s) and decay (38s) phases (see Fig 9). However, the significance of the oscillation in the impulsive phase is very low (i.e. low signal to noise ratio), it is nearly at the 99% noise level.

4 THEORETICAL INTERPRETATION

We have chosen various flaring epochs on different magnetically active stars and clearly determine the presence of QPPs (cf., Table 1). Most of the flares show periods in the decay phase ranging from ≈ 20 s to over 100s. For the 30–40s periods in the decay phase, Welsh et al. (2006) interpreted these as the sausage wave from loops of length $\sim 10^9$ cm. If we were to interpret the periods in excess of 100s as due to sausage waves, this would imply loop lengths a factor of three longer. This natural interpretation comes from the excitation of the fundamental sausage mode, possessing a definite cut-off period, in a structured cylindrical magnetic tube having appropriate density contrast with ambient background and kept almost in a field free region (Roberts et al. 1984; Edwin & Roberts 1988; Aschwanden 2004). Recently it was pointed out analytically by Lopin & Nagorny (2015) that there exists no cut-off wave-number for sausage modes of any transverse order if the plasma density outside the loop decreases only mildly with distance. This could be an obvious scenario in stellar flaring regions as diffused multiple post loop-flare loop arcades may be involved. Therefore, traverse plasma structuring across these diffused post-flare loop systems, where oscillations are excited, may not be established. Such a cut-off free environment may lead to excitation of any period related to the fundamental sausage waves. Therefore, the observed range of periods as detected in terms of flux modulations in the post flare phase, may be associated with the sausage mode waves.

AF Psc shows an event where the pre-flare had a decreasing period with amplitude. This could suggest that this period is globally present before the flare was triggered. The external periodic wave driver of the longer period propagates towards the flare current-sheet, leading to the high frequency QPPs which could be due to the dispersive evolution or resonant filtering (Santamaria et al. 2015).

Based on the solar analogy, we describe possible mechanisms behind the generation of such QPPs. We consider only those powers and associated periodicities as appeared in EMD and wavelet plots as global oscillations when they repeat > 3 cycles. Otherwise, we consider the evolution of the power associated with localized oscillations due to any transient activity in the flare, e.g., elementary reconnection.

Solar flares show QPPs at all energies, e.g. Nakariakov et al. (2010) reported on oscillations up to

energies of 2-6 MeV. These authors suggested that the time variability was due to the charge particle acceleration process, i.e. periodic magnetic reconnection. There are two possibilities here; spontaneous reconnection due to internal plasma properties and periodically triggered reconnection by perhaps MHD waves (Nakariakov & Melnikov 2009).

In some instances the power in these flares is highly localized indicating it is not a global distribution (< 3 cycle) producing the evolution of the MHD waves. Based on the analogy suggested above, it is possible that these QPPs are triggered by a periodicity in the inflow in the flare current sheet driving the periodic reconnection leading to a periodic production of non-thermal particles during the flare rise. This further generates the quasi-periodic modulation in the observed emissions (Nakariakov et al. 2006). The external wave driver in the vicinity may be playing a role in triggering oscillations in the flaring region in its rising phase (McLaughlin et al. 2009). The triggering mechanism describes that an oscillatory disturbance reaching the X-point of the flare current sheet may periodically trigger the reconnection rate causing the modulation in the emission during the rise phase of the flare (Nakariakov et al. 2006). A resistive X-point in the flaring region may go to a damped oscillatory regime of the reconnection, in which the angle between the X-point field lines, where flare maximizes, may change periodically. Therefore, these waves are found to be the fast waves of which the period is determined by the Alfvén speed profile around the X-point forming the resonator, generating the multi-periodic QPP around the peak of the flare (Craig & McClymont 1991). This is similar to the work by Takasao & Shibata (2016) who showed QPPs could be spontaneously excited by above-the-loop-top oscillations controlled by the back-flow of the reconnection outflow.

As a variation to the above, the detected periodicities in the flares may be best described as due to an avalanche of periodic bursts that occur at time intervals that correspond to the detected periods. The process could be analogous to the interacting loop model proposed by Emslie (1981) to explain the hard X-ray (HXR) bursts observed in solar flares. Given the correspondence of HXRs with white-light continuum emission, this analogy may indeed be appropriate. Phillips et al. (1992) has presented evidence to show that the continuum often observed in IUE SWP (1150-1950 Å) spectra during flares on dMe stars results from the excitation of silicon recombination radiation by intense ultraviolet lines, particularly the C IV doublet at 1550 Å. Previous work has already shown that this applies to solar flares, for which ultraviolet line emission in the transition region excites neutral silicon in or near the temperature-minimum region (Doyle & Phillips 1992).

An impulsive energy release could generate a disturbance that would travel at a speed close to the Alfvén speed. If we assume an Alfvén speed of approximately 50 km s^{-1} (i.e. the plasma derives from the upper chromosphere, see Section 1), we derive a spatial separation of $D = 50 \times T$ for the interacting loops (T is the detected period). With $T \sim 30$ sec, this indicates a separation of the order of ~ 1500 km. The spectral types of the flare stars analysed here are very similar but perhaps a way of finding evidence for or against this process is to observe flares from a range of objects of different spectral types. Flares on earlier spectral types

Table 1. A list of the flares observed by Galex, their start time, the flare duration in seconds, the derived period based on the wavelet and Empirical Mode Deconvolution in seconds (see text for the timing of these different periods).

Name	Sp. T.	Filter	Flare date	Start time	Duration (s)	Wavelet periods (s)	EMD periods (s)
AF Psc	dM4.5	NUV	2004-10-12	19:27:33	1200	30 & 120	25 & 120 & 80
CR Dra (epoch 5)	dM5.5	NUV	2005-05-05	00:59:57	512	43	40 & 50
CR Dra (epoch 12)	dM5.5	NUV	2005-07-29	13:55:22	316	43 & 20	20 & 70 & 80
CR Dra (epoch 25)	dM5.5	NUV	2009-05-25	06:30:27	512	60 & 100
GJ 3685A	dM4	NUV	2004-04-20	22:50:46	300	36 & 60 & 110	30
GL 65	dM5.5	NUV	2005-11-18	22:19:47	596	46 & 25	40
SDSS J084425.9+513830	dM	NUV	2005-01-09	22:43:22	200	40 & 120	35 & 120
SDSS J144738.47+035312.1	dM	NUV	2004-06-03	10:31:39	350	48	20 & 38

may have longer periods than those on later spectral types, in which case the flare loop separation should be different in different spectral types.

5 DISCUSSION AND CONCLUSIONS

In the present paper, we observe a range of fast quasi-periodic pulsations (20 – 120s; QPPs) in stellar flares of various magnetically active stars (e.g., AF Psc, CR Dra, GJ 3685A, Gl 65, SDSS J084425.9+513830 and SDSS J144738.47+035312.1) in the NUV filter as observed by GALEX. These QPPs provide evidence of various physical processes occurring in the observed stellar flares. Many of these flares are most likely triggered by external drivers creating a periodic reconnection in the flare current sheet and generating QPPs especially in their rising and peak phases. Some of these flares also show fast QPPs in their decay phase, indicating the presence of magnetoacoustic mode oscillations either driven externally by periodic reconnection, or intrinsically in the post-flare loop system during the flare energy release. It is possible that the oscillatory reconnection interpretation does not have to apply only to the impulsive phase as some heating is probably ongoing during the decay phase as well.

Our analyses of multiple samples of stellar flares provide signatures about externally driven periodic reconnection, associated evolution of fast MHD pulsation, and intrinsically evolved fast MHD modes in the stellar post flare loop system. Such physical processes are well known in the case of solar flares though, however, not very well established in stellar flares (Nakariakov & Melnikov 2009; Van Doorselaere et al. 2016). We analysed the evolution of oscillatory powers associated with various QPPs in the observational time-domain of stellar flares, their nature, and their possible linkage with each other, if any. Additional investigations must be specifically planned to understand the various flaring epoch of an individual magnetically active star to further understand the dynamical plasma and wave processes there.

An important finding in this work is the difference between a wavelet and the EMD analysis. In many instances, similar results were obtained. Interestingly, Gl 65 and GJ 3685A (and AF Psc) have the largest amplitude flares and unlike flares on the other stars they have coloured (pink and reddish) noisy components while the wavelet only has white noise included. Another interesting point is that almost all

flares have two different gradients in the decay phase, which is consistent with the empirical template of a stellar flare, proposed by Davenport et al. (2014). We should also note the appearance of low frequency peaks, followed by higher frequency modes. In addition, some of the peaks have a frequency ratio consistent with subharmonics. This is particularly evident, for instance, in the wavelet map of Gl 65.

ACKNOWLEDGEMENTS

Armagh Observatory and Planetarium is grant-aided by the N. Ireland Department for Communities. JUS received short-term funding from Queens University Belfast. AKS acknowledges the RESPOND-ISRO (DOS/PAOGIA205-16/130/602) project, the SERB-DST project (YSS/2015/000621) grant, and Advanced Solar Computational & Analyses Laboratory (ASCAL). MS acknowledges support from "Progetti di ricerca INAF di Rilevante Interesse Nazionali" (PRIN-INAF) 2014. We also acknowledge support from the International Space Science Institute for the team "Quasi-periodic Pulsations in Stellar Flares: a Tool for Studying the Solar-Stellar Connection". AA acknowledges support from the Science Fund of Sofia University (grant No. 80-10-229/2017). DYK acknowledges the support of the STFC consolidated grant ST/L000733/1.

REFERENCES

- Anfinogentov S., Nakariakov V. M., Mathioudakis M., Van Doorselaere T., Kowalski A. F., 2013, *ApJ*, **773**, 156
- Aschwanden M. J., 2004, *Physics of the Solar Corona. An Introduction*. Praxis Publishing Ltd
- Balona L. A., Broomhall A.-M., Kosovichev A., Nakariakov V. M., Pugh C. E., Van Doorselaere T., 2015, *MNRAS*, **450**, 956
- Benz A. O., 2008, *Living Reviews in Solar Physics*, **5**, 1
- Cho I.-H., Cho K.-S., Nakariakov V. M., Kim S., Kumar P., 2016, *ApJ*, **830**, 110
- Craig I. J. D., McClymont A. N., 1991, *ApJ*, **371**, L41
- Davenport J. R. A., et al., 2014, *ApJ*, **797**, 122
- Doyle J. G., Phillips K. J. H., 1992, *A&A*, **257**, 773
- Edwin P. M., Roberts B., 1988, *A&A*, **192**, 343
- Emslie A. G., 1981, *Astrophys. Lett.*, **22**, 41
- Kolotkov D. Y., Anfinogentov S. A., Nakariakov V. M., 2016, *A&A*, **592**, A153
- Lopin I., Nagorny I., 2015, *ApJ*, **810**, 87
- Maehara H., et al., 2012, *Nature*, **485**, 478
- Martin D. C., et al., 2005, *ApJ*, **619**, L1

- Mathioudakis M., Seiradakis J. H., Williams D. R., Avgoloupis S., Bloomfield D. S., McAteer R. T. J., 2003, [A&A](#), **403**, 1101
- Mathioudakis M., Bloomfield D. S., Jess D. B., Dhillon V. S., Marsh T. R., 2006, [A&A](#), **456**, 323
- McLaughlin J. A., De Moortel I., Hood A. W., Brady C. S., 2009, [A&A](#), **493**, 227
- McLaughlin J. A., Verth G., Fedun V., Erdélyi R., 2012, [ApJ](#), **749**, 30
- Million C., et al., 2016, [ApJ](#), **833**, 292
- Mitra-Kraev U., Harra L. K., Williams D. R., Kraev E., 2005, [A&A](#), **436**, 1041
- Nakariakov V. M., 2007, [Advances in Space Research](#), **39**, 1804
- Nakariakov V. M., Melnikov V. F., 2009, [Space Sci. Rev.](#), **149**, 119
- Nakariakov V. M., Foullon C., Verwichte E., Young N. P., 2006, [A&A](#), **452**, 343
- Nakariakov V. M., Foullon C., Myagkova I. N., Inglis A. R., 2010, [ApJ](#), **708**, L47
- Pandey J. C., Srivastava A. K., 2009, [ApJ](#), **697**, L153
- Phillips K. J. H., Bromage G. E., Doyle J. G., 1992, [ApJ](#), **385**, 731
- Pucci F., Onofri M., Malara F., 2014, [ApJ](#), **796**, 43
- Pugh C. E., Nakariakov V. M., Broomhall A.-M., 2015, [ApJ](#), **813**, L5
- Roberts B., Edwin P. M., Benz A. O., 1984, [ApJ](#), **279**, 857
- Russell A. J. B., Fletcher L., 2013, [ApJ](#), **765**, 81
- Santamaria I. C., Khomenko E., Collados M., 2015, [A&A](#), **577**, A70
- Simões P. J. A., Hudson H. S., Fletcher L., 2015, [Sol. Phys.](#), **290**, 3625
- Srivastava A. K., Lalitha S., Pandey J. C., 2013, [ApJ](#), **778**, L28
- Takasao S., Shibata K., 2016, [ApJ](#), **823**, 150
- Torrence C., Compo G. P., 1998, [Bulletin of the American Meteorological Society](#), **79**, 61
- Van Doorselaere T., De Groof A., Zender J., Berghmans D., Goossens M., 2011, [ApJ](#), **740**, 90
- Van Doorselaere T., Kupriyanova E. G., Yuan D., 2016, [Sol. Phys.](#), **291**, 3143
- Welsh B. Y., et al., 2006, [A&A](#), **458**, 921